Investigation of pitch angles on the aerodynamics of twin-VAWT under staggered arrangement

Yaoran Chen [a], Limin Kuang [a], Jie Su [a], Dai Zhou [a,b,c], Yong Cao [a], Hao Chen [a], Zhaolong Han [a,b,c,d,*], Yongsheng Zhao [a,d], Shixiao Fu [a,b,d]

[a] State Key Laboratory of Ocean Engineering, School of Naval Architecture, Ocean & Civil Engineering, Shanghai Jiao Tong University, Shanghai, 200240, PR China
[b] Key Laboratory of Hydrodynamics of Ministry of Education, Shanghai Jiao Tong University, Shanghai, 200240, PR China
[c] Shanghai Key Laboratory for Digital Maintenance of Buildings and Infrastructure, Shanghai Jiao Tong University, Shanghai, 200240, PR China
[d] Institute of Polar and Ocean Technology, Institute of Marine Equipment, Shanghai Jiao Tong University, PR China

ARTICLE INFO

ABSTRACT

The potential applications of twin vertical axis wind turbines (VAWTs) in oceanic wind energy harvesting have drawn increasing attention. Previous researches have focused on the influence of relative location, rotational direction, tip speed ratio, etc. on the power output of this system. However, limited studies have been done to uncover the effect of pitch angles on their aerodynamic performance, especially under staggered arrangements where the blade-vortex interaction remarkably occurs. In the current study, the methods of computational fluid dynamics are used to simulate the changes of power coefficients of the twin staggered H-rotors with their pitch angles. With a relative distance of 1.6 times diameter and a relative angle of 30 °, the rotors are operated at the optimal tip speed ratio in a co-rotating direction. Totally 49 cases are conducted to investigate the pitch angle range from $-6°$ to $0°$ in both rotors. It is found that the changes in pitch angle of the target rotor will affect the performance of itself and the other rotor with fixed pitch angle. Within the specified pitch range, due to the influence of the other rotor, the largest difference in power performance reaches 4.79% for the upstream rotor, and 7.04% for the downstream one. In addition, the aerodynamic mechanism is comprehensively analysed through the comparisons among velocity, vorticity and pressure fields. The findings of the current study is helpful to provide suggestions for the design of twin-VAWT system.

1. Introduction

Wind energy is believed to welcome an accelerated growth in the next two decades, reaching an installed capacity of 114.9 GW by 2030 (Jiang et al., 2020). Compared with the widely used horizontal axis wind turbines (HAWTs), the vertical axis wind turbines (VAWTs) are considered to better fit the marine environment. The gravity centre of VAWT is low and enjoys simple structure, which will facilitate the installation and maintenance (Rezaeiha et al., 2017). Moreover, the VAWT has no rigorous restrictions for the ambient environment, such as the inflow direction or turbulent condition, making it more adaptive to the complex oceanic wind than its HAWT counterparts (Peng et al., 2020).

The proposed twin-VAWT is a novel wind power concept, especially under marine environment (Jiang et al., 2020), with the typical project named Industrialization Setup of a Floating Offshore Wind turbine (INFLOW) in European Union, where two turbines of the twin-VAWT are placed at a single floater, as shown in Fig. 1 (INFLOW, 2015). The concept took the advantage of the synergic wake interactions of VAWTs to enhance the power performance (Ahmadi-Baloutaki et al., 2016). As a result, it could increase the power density of VAWTs in wind farm scenarios (Lam and Peng, 2017), and save the budget of the foundation in the case of offshore usage.

So far, the investigations of twin VAWTs have involved various aspects of the system, including the relative location (i.e. relative angle (R_d) and relative distance (φ)) and the rotational direction. Dabiri (2011) investigated the performance of counter-rotating twin VAWTs through field site measurements, and revealed that the enhanced region of φ ranging from 30 ° to 45 ° for R_d is close to 1.5D (D is the rotor diameter). Under such arrangement, Zanforlin et al. (Zanforlin and
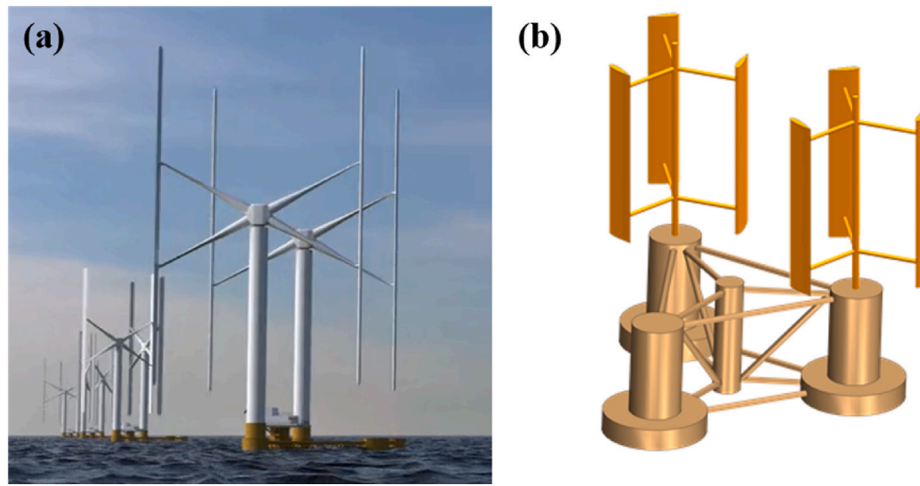
Fig. 1. 3D view of the twin-VAWT in INFLOW project (floating platform is not modelled in this work): (a) INFLOW site scene (INFLOW, 2015); (b) 3D model of this study.
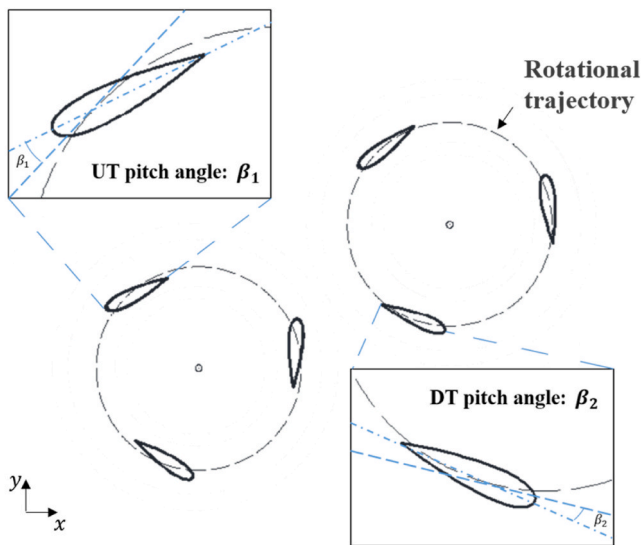

Fig. 2. Illustration of the blade pitch angles of twin VAWTs.

Nishino, 2016) identified the flow mechanisms for performance improvements by comparing different pairs of staggered twin rotors based on unsteady Reynolds Averaged Naiver Stokes (URANS) analysis. The authors concluded that the main reason for the enhancement was the blockage effects between turbines, which is in agreement with the hypothesis made by Kanner et al. (2016) and Posa (2019) in the Large-eddy simulation. In addition, for co-rotating rotors, Sahebzadeh et al. (2020) numerically studied the relationship between the layout and their individual and averaged power coefficients, and found that the pattern of overall performance was dominated by the downstream rotor, which is similar to Dabiri's findings on counter-rotating rotors (Dabiri, 2011), and the positive region occurred from φ larger than 30 ° with R_d over 1.5D. In their study, it is believed that the blade-vortex interaction and the coupled wake interaction were also the potential factors having influence on the power output, especially for downstream VAWT.

The above parameters are only related to the features of the twin VAWTs (They described the relationship **between** turbines, and became meaningless for a single turbine, for instance, there should be no difference between two isolated rotors rotating in reverse directions). Besides, some features of the single turbine were also important when it was doubled, such as the tip speed ratio (TSR) and solidity, which have

also been investigated in a few studies (Chen et al., 2017). Tavernier et al. (De Tavernier et al., 2018) showed that in the arrangement of parallel proximity, compared with the isolated one, the enhancement of twin VAWTs is still applicable for all combinations of TSR and solidity. Moreover, the research of Peng et al. (2020) showed that the rotor solidity would have a dominant effect on the rated TSR of its parallel twin system, and the lower the solidity, the higher the rated TSR. Besides, combined with the results obtained from the work of Zanforlin et al. (Zanforlin and Nishino, 2016), the optimal TSR for twin VAWTs was found to be different (right-shifted) from their standalone counterparts.

However, limited researches exhibited the effect of another critical parameter of the twin-VAWT system, i.e., the pitch angle (Yang et al., 2018). This parameter is more convenient for real-time control than the relative location in engineering, especially for VAWTs with fixed foundations. As one of the limited studies, the study of Peng et al. (2020) revealed the strong effect of pitch angle on averaged power coefficient. However, the object it studied was a strict twin system in a parallel layout (the same as those in other studies (Chen et al., 2017)), in another word, the two turbines are identical. Among their test cases, the pitch angles of the two VAWTs changed synchronously. This leaves a gap in how the pitch scheme would develop into incongruity when the layout was not symmetric, namely, under staggered placement or the inlet direction inclined. In addition, the incompatibility in the pitches of upstream and downstream turbines (UT and DT) could become more distinct and influential when they were placed in proximity, and strong blade vortex interaction (BVI) could happen, as suggested by Sahebzadeh et al. (2020).

Therefore, in this work, investigations of the influence of pitch angles on staggered twin VAWTs are systematically conducted. Considering the critical wake boundary of the upstream rotor based on former researches (Dabiri, 2011) (Sahebzadeh et al., 2020), the relative distance between two turbines is set as 1.6D, and the relative angle is 30°. The two turbines are identical in terms of the rotational direction, starting phase and angular velocity. The high-fidelity computational fluid dynamics (CFD) methods are used to predict the power performance of both rotors and their average, with which the contour maps with axes of pitch angles are plotted. More importantly, the corresponding mechanism is analysed through comparisons and discussions of the power coefficients, instantaneous moments as well as the velocity, vorticity and pressure fields.

The rest parts of this article are constructed as follows. In Section 2, the description of test cases is presented. In Section 3, the CFD methods and validation are given. In Section 4, the numerical results and multi-aspect discussions on findings are elaborated. At last, in Section 5, solid conclusions are drawn.

Table 1
Geometrical characteristics of each rotor in twin VAWT system.

Diameter (D)	1030 mm	Blade Profile	NACA0021
Blade Number (N)	3	Chord length (c)	85.8 mm
Blade Span (h)	1456.4 mm	Solidity (σ)	0.25
Range of pitch changes		$[0°, -1°, -2°, -3°, -4°, -5°, -6°]$ (for both UT β_1 and DT β_2)	

2. Problem setup

The test cases of this work are performed based on a system of two staggered straight-blade VAWTs with different pitch angles. As shown in Fig. 2, the blade pitch of the VAWT is defined as the angle between the blade chord line and the tangential line of the rotational trajectory, taking toe-out as negative. In this article, the pitch angle of the upstream turbine is denoted by β_1, and that of the downstream turbine is denoted by β_2. Both β_1 and β_2 have the same range varying from $-6°$ to $0°$ with the step of $1°$. Therefore, the total number of cases with different combinations of β_1 and β_2 equals $7^2 = 49$.

The geometrical parameters of each VAWT in the current dual system are listed in Table 1. The model was chosen for two reasons. First, its aerodynamic performance has been both experimentally and numerically studied in previous researches, such as the researches by Castelli et al. (Raciti Castelli et al., 2010) and Ni et al. (2021a), which is suitable to be used as the reference. Second, the aspect ratio (h/c) of the blades is high, reaching about 17. According to Rezaeiha's conclusion (Rezaeiha et al., 2018a), it can sufficiently mitigate the 3D blade tip effects when merely conducting 2D analysis on the plane of mid-span, thereby largely saving the computational budget.

In the current study, the investigations are conducted by using the 2D computational fluid dynamics (CFD) method. Taking the zero-pitch arrangement as an example, the panel layout of the computational model of the target twin-VAWT system is shown in Fig. 3. As mentioned in Section 1, the relative distance between rotors is 1.6D (D: turbine diameter of 1.03 m), and the relative angle is 30°. The distance between the center of the upstream turbine and the velocity inlet (9 m/s) is 10D, while the distance between the pressure outlet (0 Pa) and the center of downstream turbine is set at 15D to make the far wake fully developed. Considering the blockage effect and the symmetricity for dual turbines, the distance between the side edge and its nearest rotor is 10D, making the blockage ratio less than 5% (Sahebzadeh et al., 2020). The shear stress condition for both sides is slip-wall, while all blade surfaces are

non-slip wall.

The turbine blades are placed in ringlike domains, whose boundaries divide the entire domain into stationary (outside) and rotational (inside) parts. The inner diameter of the ring is 0.7 m (0.68 D), and the outer diameter is 1.4 m (1.36 D). Such interval has been proven to be sufficient for mesh meshing and aerodynamic performance prediction of VAWTs (Su et al., 2020a). The above set-up is congruously applied to all dual-VAWT cases and the solo VAWT case (as the baseline) for model validation.

3. CFD methods and simulation validation

The CFD investigations will be presented in this section. In Section 3.1, the numerical settings (including the turbulence model) will be introduced. In Section 3.2, taking the solo turbine as an illustration, the mesh settings (including the convergence test by grid convergence index (GCI) (Roache, 1997a)) will be presented. In Section 3.3, to verify the reliability of above settings, the validation is performed through the comparison with available references.

3.1. Solver settings

As it was mentioned, the 2D CFD method was used in this work, and the numerical settings are as follows. Based on the finite volume method (FVM), the commercial software STAR-CCM+ 13.06 (Simcenter, 2018) was adopted to solve the incompressible unsteady Reynolds-Averaged Navier-Stokes (URANS) equation. The SIMPLE scheme was used to couple the pressure-velocity equation in the URANS model (Patankar, 1980). For both temporal discretization in implicit integral and the spatial discretization in the upwind format of segregated flow (convective term), the second-order accuracy was employed.

The turbulence model in this work was the two-equation Shear Stress Transport (SST) k-ω model, owing to its advantage in handling the boundary flow around the blade (Wilcox, 1998; Menter, 1994). Such model has been widely used in previous work whether for the isolated VAWT (Roache, 1997b) or dual VAWT (Naik and Tiwari, 2021) system and its feasibility to the current work will also be validated as provided in Section 3.3.

The azimuthal increment was set to be $T/360$ (i.e. 1 ° per time-step) and the maximum inner iteration was 20. Such settings were proved to be sufficient enough for investigating the general wake features and averaged power coefficient (C_p) of VAWTs (Ni et al., 2021b). The
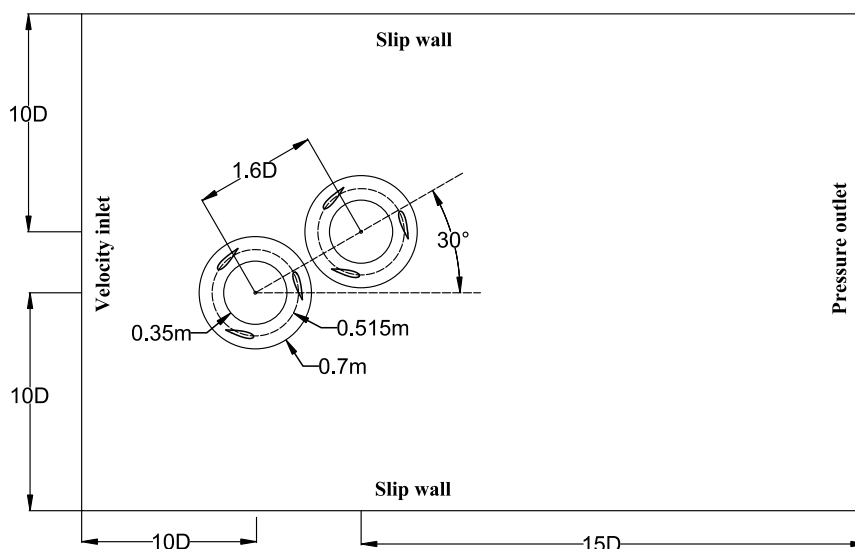

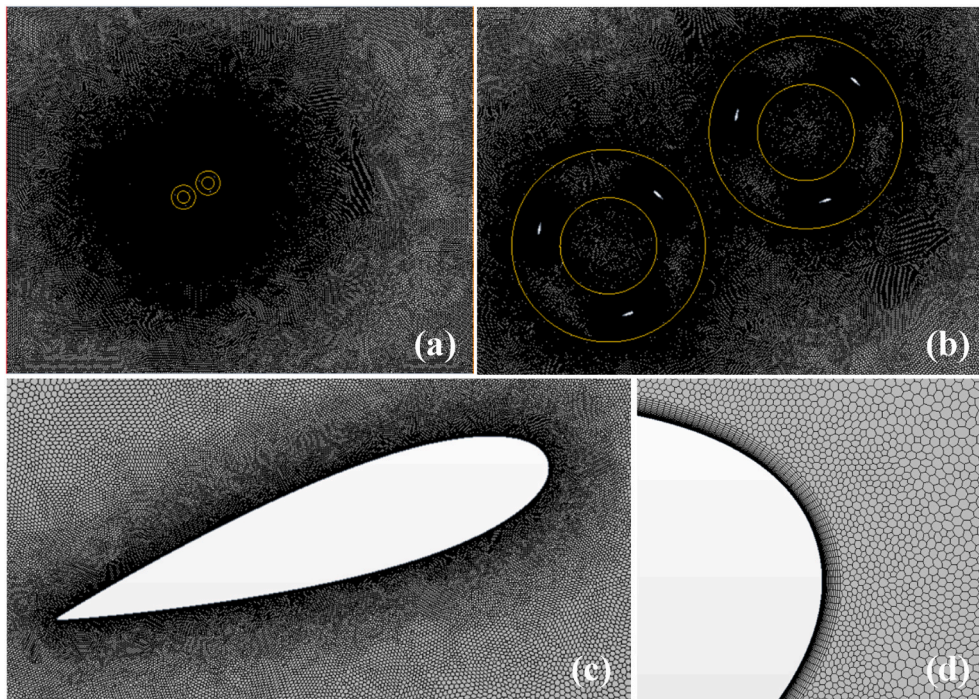**Fig. 3.** Computational domain and boundary conditions for twin VAWTs in a staggered arrangement.

Fig. 4. Mesh topology of a sample twin-VAWT numerical model (β_1: 0°, β_2: 0°): (a) Overall view; (b) Rotational domain; (c) blade vicinity; (d)leading edge.
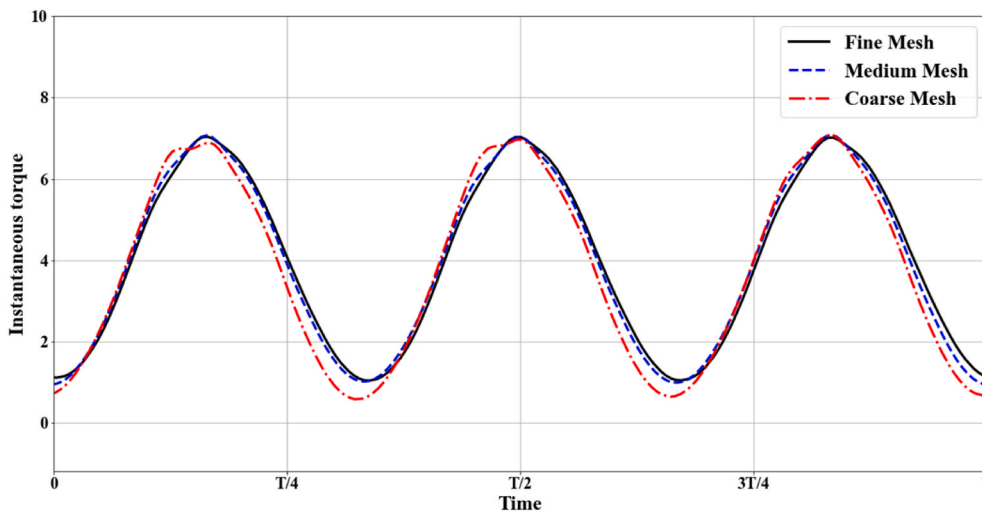

Fig. 5. Instantaneous torque during a period of three mesh schemes.

Table 2
GCI analysis of three refinements of grids.

Mesh scheme	Target cell size on the blade	Number of grids	Averaged torque (Nm)	GCI (%)
#1 (fine)	0.15 mm	668305	3.9705	1.55
#2 (medium)	0.1875 mm	561243	3.9190	3.22
#3 (coarse)	0.234375 mm	471781	3.8144	/

simulations were terminated after the physical time reaching 17 times periods, where the targeted index of performance (C_p) sufficiently converged (the error between adjacent periods less than 0.5%).

3.2. Mesh settings

The mesh settings of the CFD model are provided in this section,

including its general topology, the convergence examinations based on grid convergence index (GCI), the validations using the selected grid scheme and the solver settings. It should be noticed that the last two parts in this subsection are conducted with the solo turbine because the references for comparison mostly used individual VAWTs.
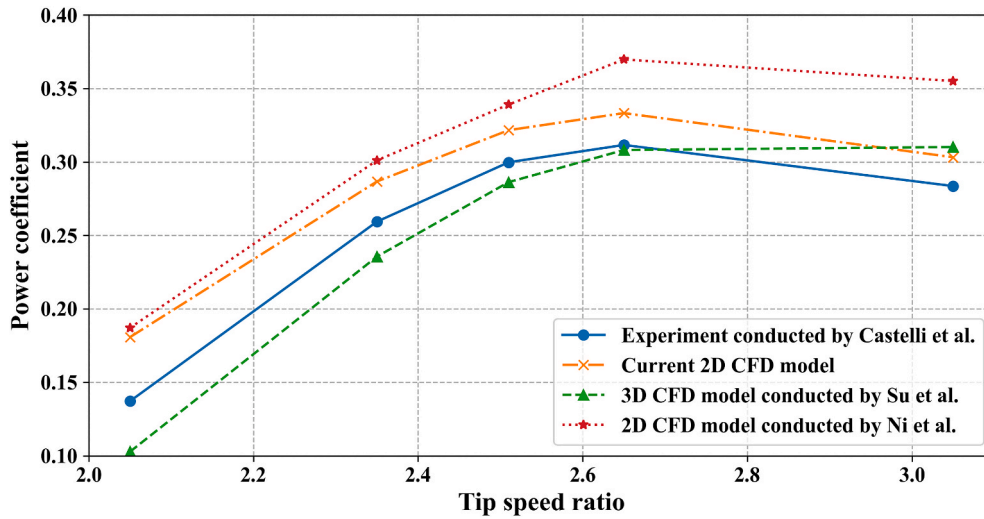
Fig. 6. CFD Model validation: comparison of the power coefficients of solo VAWT with experimental and numerical references (Raciti Castelli et al., 2010; Ni et al., 2021b; Su et al., 2020b).
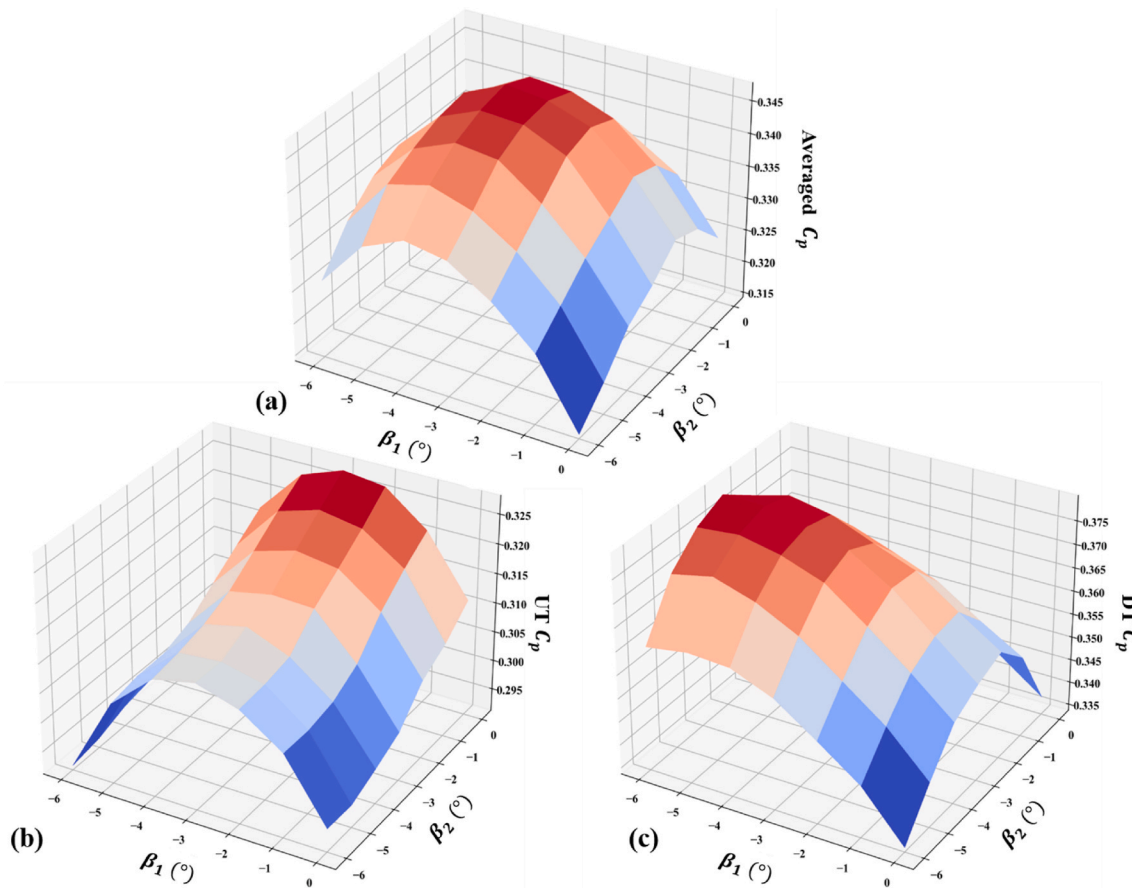

Fig. 7. Comparison of power coefficient with various pitch angle combinations: (a) Averaged power coefficient of UT and DT; (b). UT power coefficient; (c) DT power coefficient.

3.2.1. Mesh topology

To illustrate the mesh topology, Fig. 4 provides a mesh scene of a sample case from the overall view (Fig. 4(a)), the closer view of the rotational domain (Fig. 4(b)), the vicinity of the blade (Fig. 4(c)) and the leading edge (Fig. 4(d)) to show the prismatic grid layers.

As in Fig. 4, the polyhedral grids are used to build the unstructured mesh. The total number of grids is over 0.95 million, where the steady

flow field accounts for 0.3 million and the other grids are in the rotational domains. The grids across interfaces are designed to have approximately consistent sizes hence ensuring continuity (He et al., 2020). The prismatic grids are used in boundary layers of blades, whose thickness is 0.54 mm with 28 layers in total. The growth rate of the prismatic layers is 1.15 to guarantee the $y+$ less than 1, to resolve the viscous sub-layer (He et al., 2020). In specific, the maximum values of
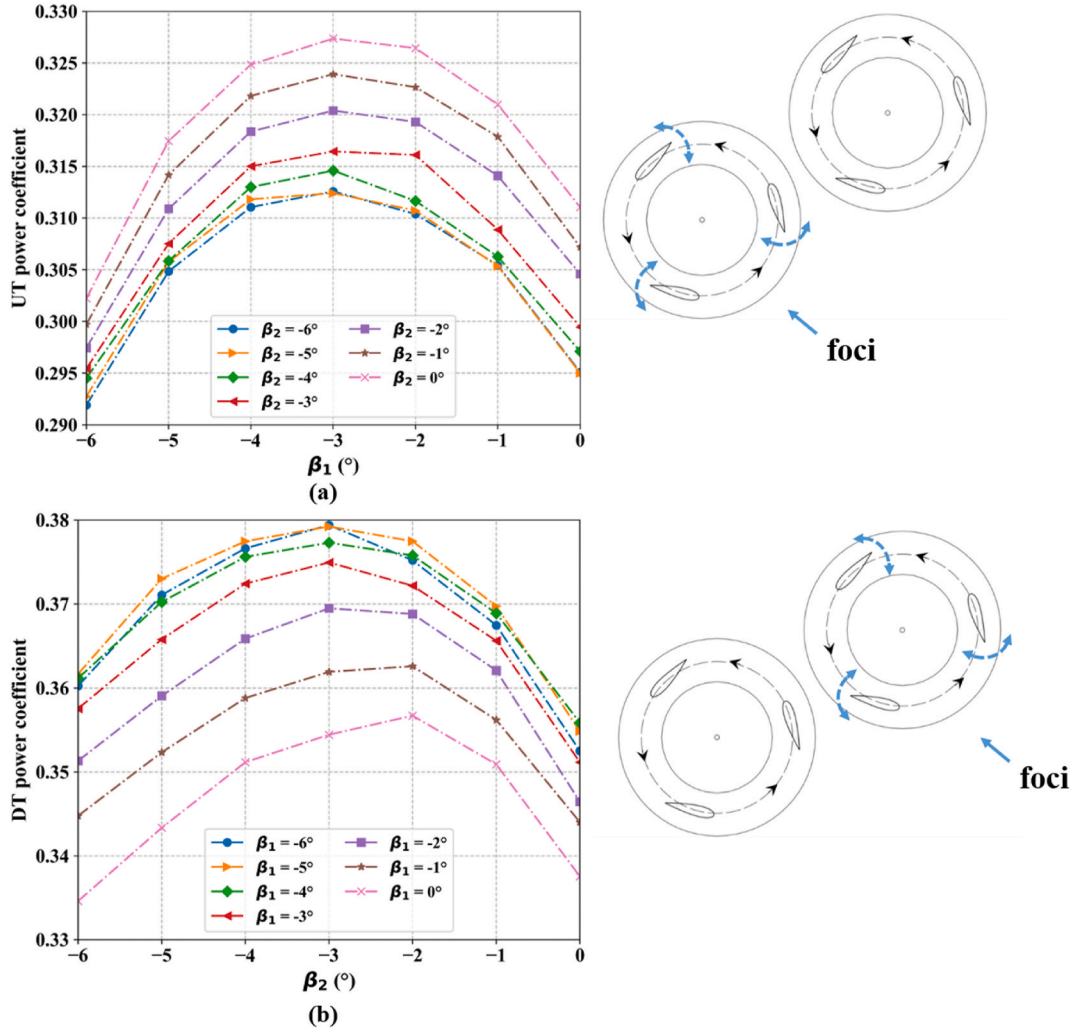
Fig. 8. Changes of performance in UT and DT when themselves pitches vary from $-6°$ to $0°$: (a). Foci on UT power coefficient as β_1 varies; (b) Foci on DT power coefficient as β_2 varies.

$y+$ are 0.308 and 0.326 for upstream and downstream turbines, respectively.

3.2.2. Gird convergence test

To test the grid-dependency of the result, a model of the solo turbine (pitch = $0°$) using the same settings (fine mesh) is made, whose total number of grids is 668,305. With a magnification factor of 1.25 to uniformly enlarge **all** grid sizes (though the real gird refinement ratio is 1.09 due to unstructured mesh), the grid number of the medium and the coarse are 561,243 and 471,781, respectively. The instantaneous torques on blades under three mesh schemes are plotted in Fig. 5. Its average value $\overline{Q}$ during the last periods is used to evaluate the simulation result.

As shown in Fig. 5, the three curves show a trend of convergence. While the overall tendencies are similar, the difference of the torque between the current mesh (fine) and medium mesh is far less than that between medium and coarse mesh, especially in the valley of the curve. The large gap of the coarse curve from others gives the lowest averaged moment (-2.67% from medium and -3.93% from fine), as Table 2, column 4 shows below:

The analysis based on the grid convergence index (GCI) (Roache, 1997b) is also shown in Table 2. According to Roache et al. (Roache, 1997b), for two-dimensional simulation, the safety factor (F_s) to calculate GCI index is set to be 1.25. The values of GCI$^{\text{fine}}$ and GCI$^{\text{medium}}$ equal to 1.55% and 3.22% respectively, getting smaller as mesh number

increases. Based on the GCI value, the asymptotic range α is equal to 0.99($\approx$1) in this test, showing that the grid refinement achieves an asymptotic range. Also, the value of convergence ratio (R) is calculated to be 0.49, showing that the grids are monotonic converged (Naik and Tiwari, 2021).

3.3. Simulation validation

The validation of the CFD model is proposed in this section. To examine the feasibility of the current model, The TSR-C_p curves of the isolated turbine with $0°$ pitch measured by Castelli et al. (experiments) (Raciti Castelli et al., 2010), Ni et al. (2D CFD test) (Ni et al., 2021b) and Su et al. (3D CFD test) (Su et al., 2020b) are used for comparison. The expression of TSR (λ) and C_p are as follows:

$$C_p = \frac{\overline{Q}\omega}{0.5A_s\rho V_\infty{}^3} \tag{1}$$

$$\lambda = \omega R/V_\infty \tag{2}$$

where ω is the angular speed of the rotor. A_s is the reference area of the rotor, equal to 1.236 m^2 according to Castelli et al. (2011). $\rho = 1.225$ kg/m^3 denotes the air density under the standard condition. $V_\infty = 9$ m/s denotes the velocity of the wind inlet.

As shown in Fig. 6, the power coefficient changes with tip speed

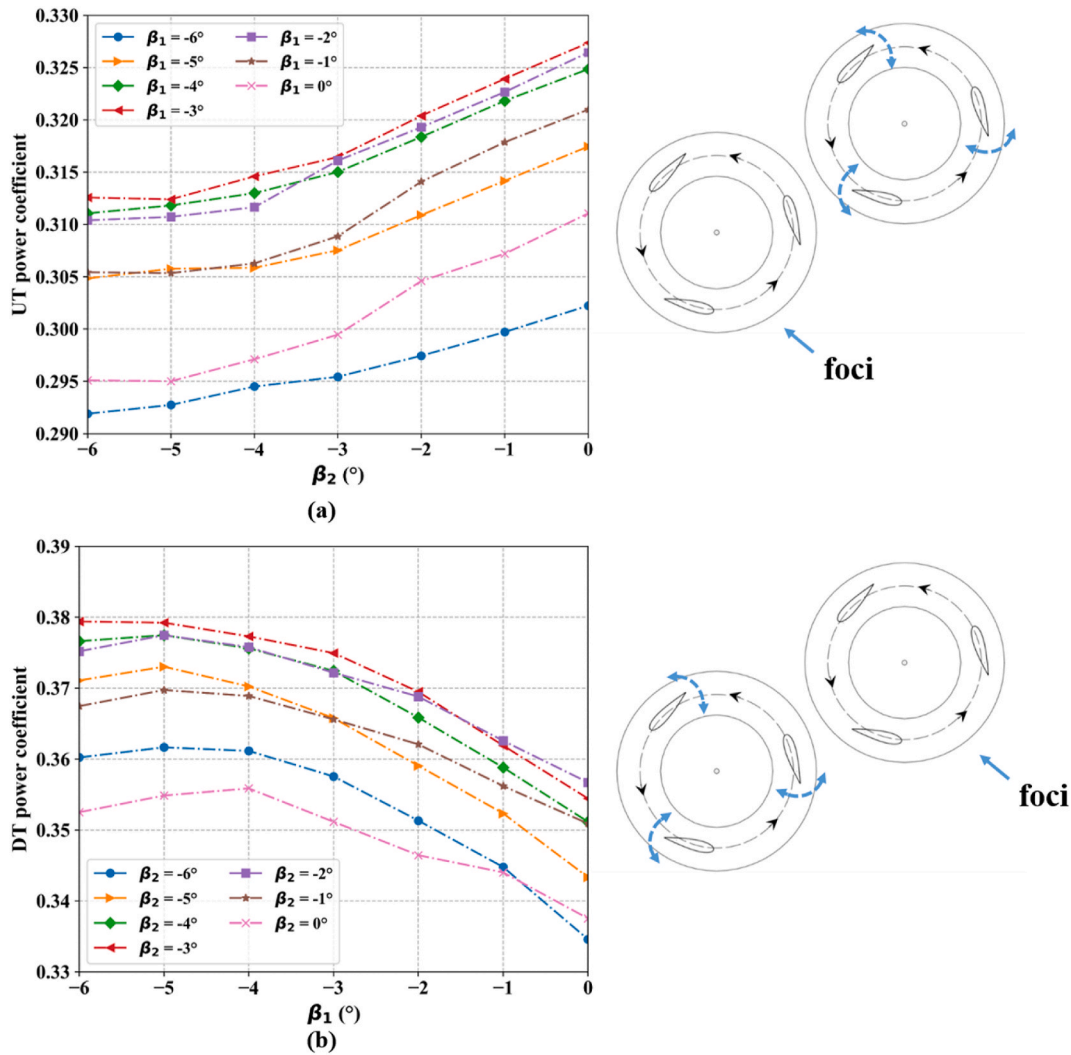**Fig. 9.** Changes of performance in UT and DT when the other turbine's pitch angle varies from $-6°$ to $0°$: (a). Foci on UT power coefficient as β_2 varies; (b) Foci on DT power coefficient as β_1 varies.

ratios ranging from 2.15 to 3.05 are plotted. As it can be found, the current model can well depict the tendency of the experimental reference, where the values are generally higher. This is partly because of the 2D simplifications and the neglecting of struts and blade surface roughness (Rezaeiha et al., 2018b). Nevertheless, it confirms that the current model is reliable to provide general power performance for the simulations in the rest parts.

The optimal TSR is equal to 2.65 with the rotational speed $\omega = 46.31$ rad/s. Under such conditions, the averaged torque of all blades for an isolated turbine measured by the current model is equal to 3.9705 Nm, corresponding to the power coefficient of 0.333 (Fig. 6, dash-dot line). The following investigations and comparisons are all under this working condition.

4. Results and discussion

The numerical results of the twin-VAWT system are shown in this section. The corresponding discussion includes the overall performance (evaluated by power coefficient), the instantaneous blade torque and various physical fields as the evidence to explain the underlying mechanism.

4.1. Performance comparison

The overall performance evaluated by using the power coefficient is provided and analysed in this subsection. As shown in Fig. 7(a), the optimal average power coefficient is obtained by the combination of $[\beta_1, \beta_2] = [-4°, -2°]$, i.e., the power coefficient of 0.347, which is 4.2% higher than the solo turbine with zero pitch. The outcome is the combination of the individual effect of the power coefficients of UT and DT, respectively. As shown in Fig. 7(b), the surface of the UT C_p is an ascent tunnel where the highest point occurs at $[-3°, 0°]$ and the lowest one is at $[-6°, -6°]$. However, in Fig. 7(c) showing the DT performance, the surface is a decent tunnel where the highest point is located at $[-6°, -3°]$ and the lowest one is at $[0°, -6°]$.

To further analyse the rules reflected by Fig. 7(b) and (c), their projections are plotted in Fig. 8 and Fig. 9 to show the trends more clearly. First, in Fig. 8, we focus on the changes of performance in UT and DT when their own pitch angles vary from $-6°$ to $0°$ (the other VAWT pitch is fixed).

As can be seen from Fig. 8(a), the curves of UT performance remain the similar parabolic trend with the change of β_2. The best points for each curve occur together when $\beta_1 = -3°$. As for DT curves, however, their shapes vary slightly under various UT pitches. The optimal β_2 is around $-2°$ when β_1 changes from $0°$ to $-2°$, and gradually recovers to $-3°$ as β_1 continues to increase to $-6°$.
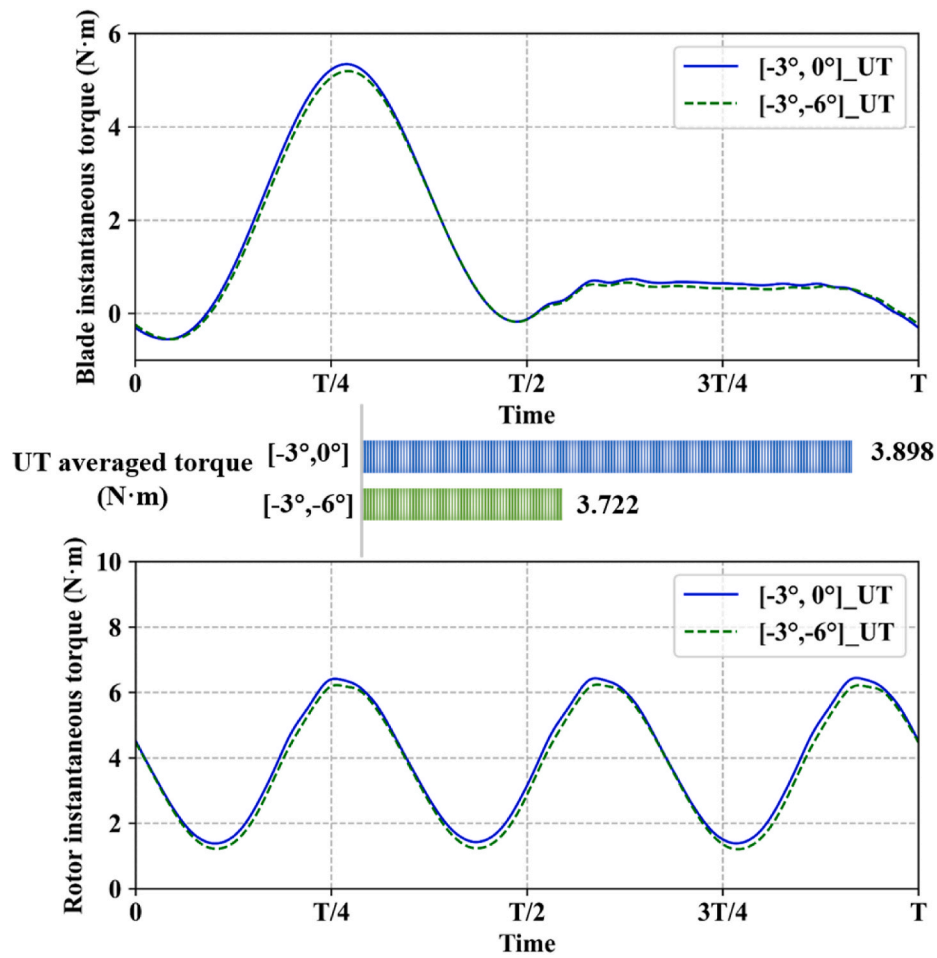
Fig. 10. Comparison of UT instantaneous blade torques between the pitch angle combinations of [−3°, 0°] and [−3°, −6°].
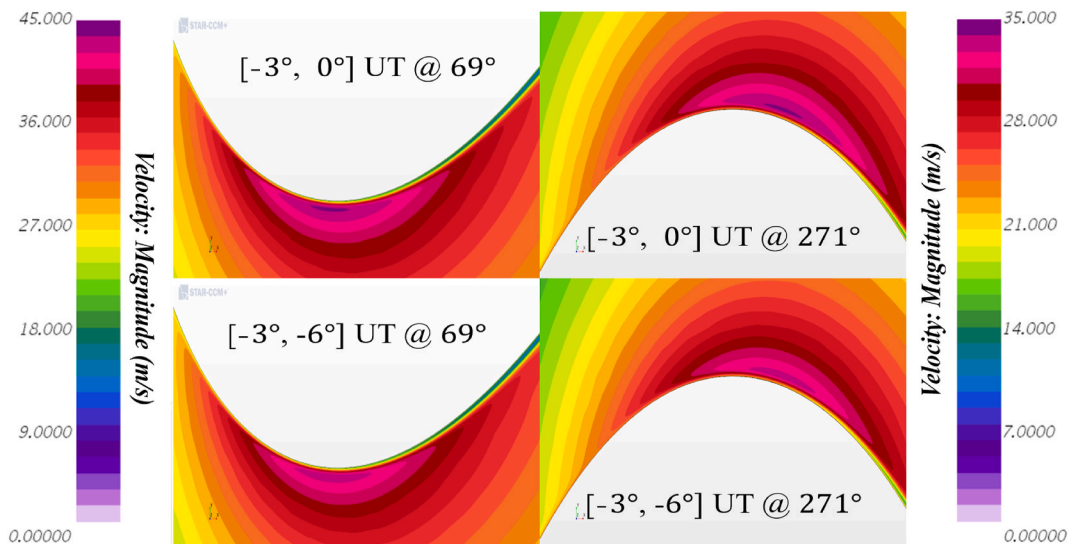

Fig. 11. Comparison of the local velocity field at the leading edge of the UT blade while β_2 changes. Left: upwind region; Right: downwind region.

Next, more importantly, we focus on the change of UT and DT performance with the change of the pitch angle of the other turbine. As can be inferred from Fig. 9, although the self-pitch remain unchanged, all the performance shows a regular and almost monotonous change as the pitch of the other turbine decreases.

In Fig. 9(a), the UT performance keeps increasing with the decrease

of the magnitude of β_2. The gradients of the curves also show a climbing trend. In general, the highest curve is observed when $\beta_1 = -3°$, and the lowest value occurs when $\beta_1 = -6°$. Furthermore, for the optimal curve, the highest point reaches 0.327 at the pitch angle combination of [−3°, 0°], and the lowest one is 0.312 at [−3°, −6°], showing a large difference of 4.80%.
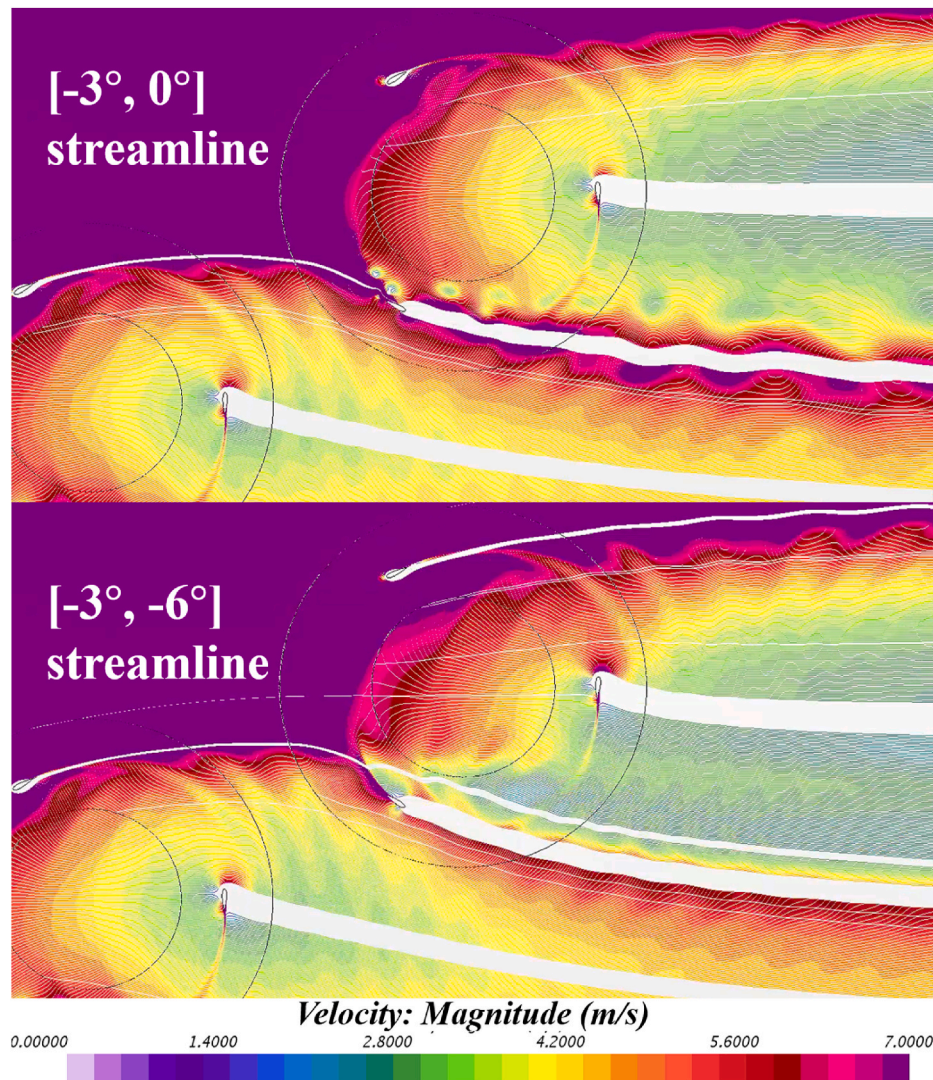
Fig. 12. Comparison of velocity streamlines around the UT blade at an azimuthal angle of 271°

In contrast, in Fig. 9(b), the DT performance gradually deteriorates when β_1 changes from $-6°$ to $0°$ for every β_2. However, similar to Fig. 9 (a), the reduction rate of DT power coefficients presents a slow-to-fast pattern. The highest curves occur when $\beta_2 = -3°$, while the lowest is observed when $\beta_2 = 0°$. Impressively, for the optimal curve, the largest difference in power performance is 7.04%; as for the pitch angle combinations, they are $[0°, -3°]$ versus $[-6°, -3°]$. To discover the underlying mechanism, typical cases are further analysed in the following sections.

4.2. Upstream turbine comparison

In this section, comparison of the UT torque curves are made, where the cases are two twin-VAWTs with the same UT pitch: $\beta_1 = -3°$, but different DT pitches: $\beta_2 = 0°$ or $\beta_2 = -6°$.

As shown in Fig. 10, under the influence of the DT blade pitch, the averaged torques of UT are 3.898 N · m and 3.722 N· m for the cases $[-3°, 0°]$ and $[-3°, -6°]$, respectively. From the instantaneous torque curves, the main enhancements of $[-3°, 0°]$ over $[-3°, -6°]$ occur at the following two episodes. In the upwind region, the improvements occur before and a little bit after the first quarter of the period, where the azimuthal angle varies from 45° to 100°. While in the downwind region, the increase happens around the third quarter of the period, where the azimuthal angle is at about 270°. In other parts of the two curves, the

instantaneous torques are generally overlapped.

To explain this phenomenon, we freeze the azimuthal angle of 69° and 271° to form an illustration. The corresponding velocity fields of UT and DT blade around the leading edge of the blade are plotted in Fig. 11, respectively. It can be found that the velocity magnitude of the local flow encountered with the toe of the UT blade for the case of $[-3°, 0°]$ is larger than that of $[-3°, -6°]$ for both upwind and downwind regions, regardless of the local maximum velocity value or the high-speed coverage, leading to a larger pressure difference between the suction side and the pressure side of the blade. Consequently, it results in a larger tangential force, and hence a larger instantaneous blade torque.

The reason why the changes of β_2 can alter the above UT local velocity field can be further explained by the streamline plotted in Fig. 12. It can be seen that when the DT blade has a pitch of 0° (see the DT blade at 151°), the velocity streamlines below it, from high-speed to low-speed, are more suppressed than that of the DT blade with a pitch of $-6°$. Consequently, the streamlines become denser and the corresponding special gradient gets larger. Therefore, general speaking, the velocity magnitude in the zone between the leading edge of the UT blade at 271° and its neighbouring DT blade is larger due to the blockage effect. In another word, at $\beta_2 = 0°$, the DT blade can further accelerate the local flow velocity beneath it due to the flattening of its shape along the inflow direction than the case when $\beta_2 = -6°$. And this can also explain the reason why UT performance shows a continuous and monotonic

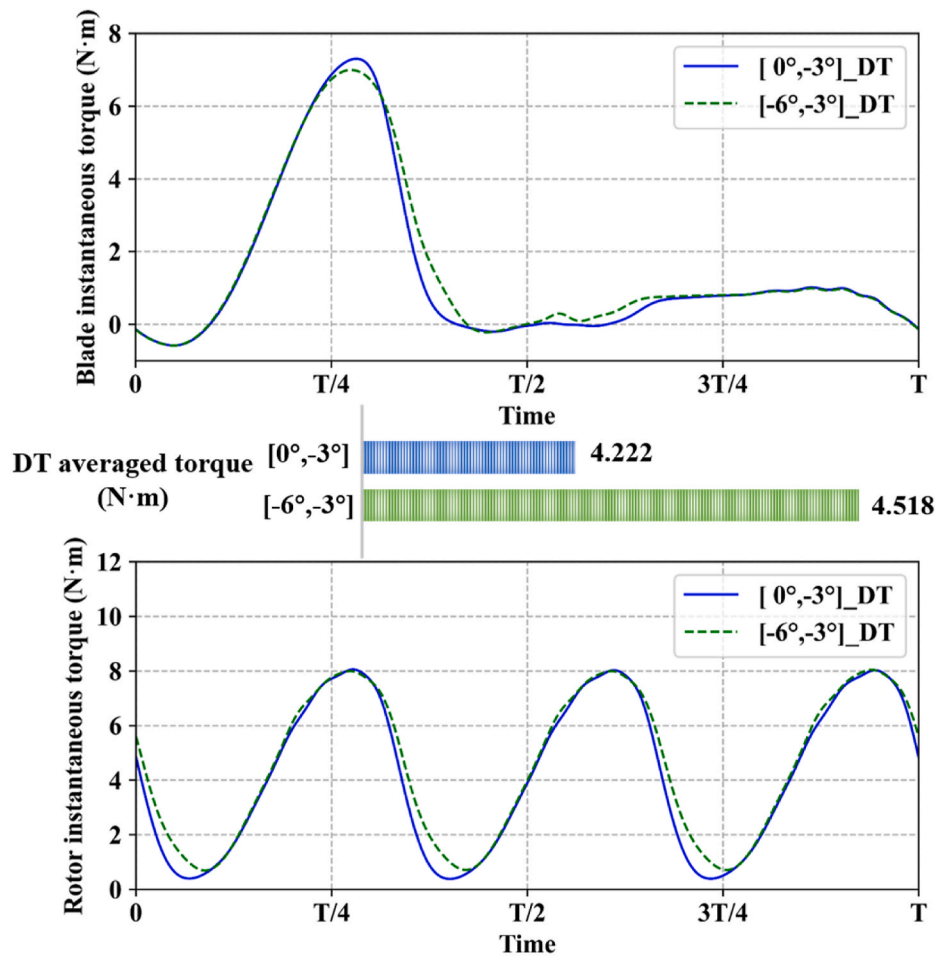**Fig. 13.** Comparison of DT instantaneous blade torques between the pitch angle combinations of [0 °, −3 °] and [-6 °, −3 °].

increase as β_2 changes from $-6°$ (the most inclined) to $0°$ (the flattest).

4.3. Downstream turbine comparison

In this section, comparison of the DT torque curves are conducted, where the two cases are twin-VAWTs with the same DT pitch, i.e., $\beta_2 = -3°$, but different UT pitches, i.e., $\beta_1 = 0°$ or $\beta_1 = -6°$.

As shown in Fig. 13, for DT cases, by changing β_1 from $0°$ to $-6°$, the averaged torque increases from 4.222 Nm to 4.518 Nm while β_2 remains $-3°$ unchanged. From the instantaneous torque curves, the improvements of DT instantaneous blade torque are mainly observed between the second and the third quarter of the period. Combined with the relative location between UT and DT (Fig. 3), it is reasonable to assume that such performance enhancement of DT is due to the change of induced flow field from the UT wake.

For illustration, in Fig. 14, we take a close look at the pressure field and the vorticity field of the DT blade at its most predominant azimuthal angle of 132°. As can be found from the pressure field, the suction area (blue) for the case of $[-6°, -3°]$ is larger than that of $[0°, -3°]$, covering more leading edge of the blade. Besides, on the pressure side (red), the area is moving backwards and away from the toe, resulting in a larger component along the axial direction and smaller one along the tangential direction. Both contribute to a larger tangential force on the blade, and hence a more instantaneous torque.

Similar evidence from the vorticity field in Fig. 14 also shows that the stagnation point (the junction of the red and blue lines near the blade surface) is moving in clockwise direction from the DT blade in [0°, −3°] case to that in [−6°, −3°]. Such movement results in more positive vortex near the leading edge of the blade. And this can benefit the local

blade rotation of DT from the azimuth angle of 90° to 180°, and both the majority of near-wall vortex and the blade's leading edge moved in the same direction, that is, positive x-direction and negative y-direction. Therefore, the resistance force is lowered, and the torque is therefore enhanced.

As shown in Fig. 15, seen from the vorticity scene in a farther view, the phenomenon in Fig. 14 is actually caused by the shedding vortex due to the UT blades (highlighted by dashed circles).

Compared with the case of [0°, −3°], the UT blades in the case of [−6°, −3°] are toe-out and tail-in. Therefore, the trajectory of its shedding wake is suppressed and flattened (as shown by the dashed and solid lines in Fig. 15(b)). Consequently, the DT blade in the case of [−6°, −3°] can evade the negative shedding vortex generated by UT blades. However, in Fig. 15(a), the corresponding DT blade is immersed in the clockwise (i.e. negative) vortex which, then causes the stagnation point to move anti-clockwise, and hence reduces the instantaneous torque of DT blade at the azimuth angle ranging from 90° to 180°. In addition, such influence regarding the shedding wake trajectory from UT also explains why the difference of the DT instantaneous torque mostly happens in the second and the third quarter of the rotation period (Fig. 13), while in other parts, the curves are nearly overlapped.

In general, the aforementioned analyses show that the mutual influence of power coefficient from the pitch angles on twin-VAWT system is mainly caused by the blockage and wake effects. In such staggered arrangement, the pitch angles of blades can significantly alter the velocity and vorticity field in the area between UT and DT, and therefore change the distribution of local pressure fields around the blade leading edges, causing differences in torque.
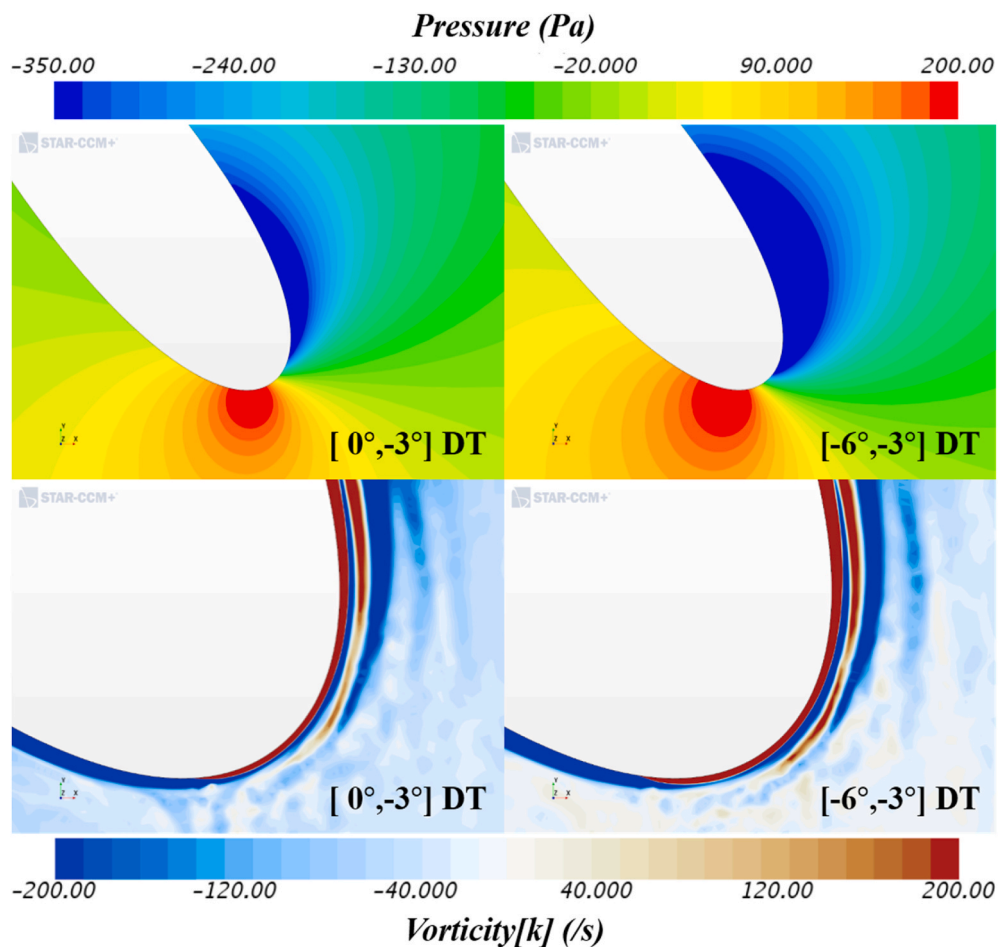
Fig. 14. Comparison of the pressure and vorticity fields around the leading edge of DT blade at an azimuthal angle of 132°

4.4. Limitations

Although the mechanism of the pitch (geometry) varying with physical field changes and eventually with the difference in the aerodynamic performance of UT and DT blades has been fully elaborated, there are two main limitations in the current work:

(i). Despite the support by the mechanism, the rules described in Section 4.1 could not be easily propagated or generalized. The relative location, the phase lag, the blade number and the blade profile of VAWT could all have a significant impact on the results of the current problem.

(ii). The range of the variation of pitch has not been designed under a careful investigation from the view of blade-flow interaction, as explained in Sections 4.2 and 4.3. In another word, how the rule will develop outside the proposed range is unknown.

5. Conclusion

This study investigated the influence of pitch angles on the performance of twin vertical axis wind turbines under a staggered arrangement. The pitch range was set to be from $-6°$ to $0°$, and the two rotors were rotating in co-direction at their best tip speed ratio. The most novel contribution of this study is that the changes in pitch angle of one rotor will also affect the performance of the other, although its pitch remains fixed. The rules were revealed, and the aerodynamic mechanism was proposed, with main conclusions summarized as follows:

First, for the UT performance under the influence of β_2, the UT power coefficient was enhanced with the decrease of the magnitude of β_2, by a maximum percentage of around 4.7% over the designed range. This was due to the fact that more flattened shape of the DT blade can accelerate the flow field between turbines. Second, for the DT performance under the impact of β_1, the DT power coefficient was increased with the increase of the magnitude of β_1, by an impressive maximum percentage of around 7.1% over the designed range. Differently, this was caused by the variant of shedding wake trajectory as β_1 changes, and a more tail-in pitch would suppress the wake width, and therefore let the DT blade evade the negative vortex during the second to the third quarter of the period.

The above findings are beneficial to the design and real-time control of the twin-VAWT system, especially at a fixed location. Moreover, the mechanism proposed may provide reference and information for scientific and engineering researches of twin VAWTs.

CRediT authorship contribution statement

Yaoran Chen: Investigation, Methodology, Software, Writing, Data curation, Writing – review & editing. **Limin Kuang:** Methodology, Writing – review & editing. **Jie Su:** Methodology. **Dai Zhou:** Writing – review & editing. **Yong Cao:** Supervision, Writing – review & editing. **Hao Chen:** Writing – review & editing. **Zhaolong Han:** Supervision, Writing – review & editing. **Yongsheng Zhao:** Supervision, Writing – review & editing. **Shixiao Fu:** Supervision, Writing – review & editing.

Declaration of competing interest

The authors declare that they have no known competing financial interests or personal relationships that could have appeared to influence
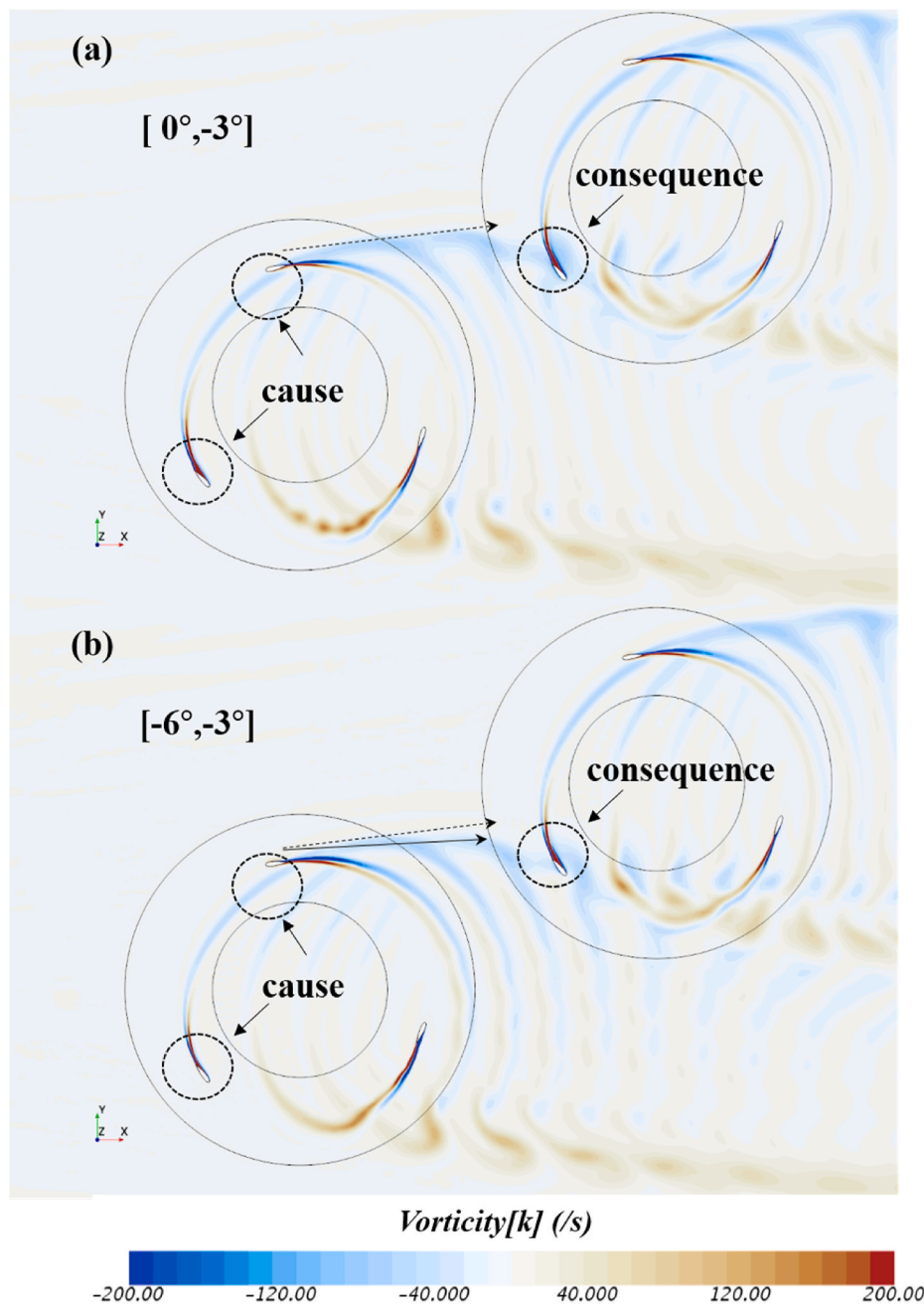
Fig. 15. Comparison of the vorticity fields between cases $[0°, -3°]$ and $[-6°, -3°]$ causing an instantaneous torque improvement for DT blade at an azimuth of $132°$.

the work reported in this paper.

Appendix A. Supplementary data

Supplementary data to this article can be found online at https://doi.org/10.1016/j.oceaneng.2022.111385.

References

Ahmadi-Baloutaki, M., Carriveau, R., Ting, D.S., 2016. A wind tunnel study on the aerodynamic interaction of vertical axis wind turbines in array configurations. Renew. Energy 96, 904–913.

Castelli, M.R., Englaro, A., Benini, E., 2011. The Darrieus wind turbine: proposal for a new performance prediction model based on CFD. Energy 36 (8), 4919–4934.

Chen, W.H., Chen, C.Y., Huang, C.Y., Hwang, C.J., 2017. Power output analysis and optimization of two straight-bladed vertical-axis wind turbines. Appl. Energy 185, 223–232.

Dabiri, J.O., 2011. Potential order-of-magnitude enhancement of wind farm power density via counter-rotating vertical-axis wind turbine arrays. J. Renew. Sustain. Energy 3 (4), 43104.

De Tavernier, D., Ferreira, C., Li, A., Paulsen, U.S., Madsen, H.A., 2018. June). Towards the understanding of vertical-axis wind turbines in double-rotor configuration. In: Journal of Physics: Conference Series, 1037. IOP Publishing, p. 22015, 2.

He, J., Jin, X., Xie, S., Cao, L., Wang, Y., Lin, Y., Wang, N., 2020. CFD modelling of varying complexity for aerodynamic analysis of H-vertical axis wind turbines. Renew. Energy 145, 2658–2670.

INFLOW. Industrialization Setup of a floating offshore wind turbine. Available online: https://www.inflow-fp7.eu/. (Accessed 25 January 2015).

Jiang, Y., Zhao, P., Stoesser, T., Wang, K., Zou, L., 2020. Experimental and numerical investigation of twin vertical axis wind turbines with a deflector. Energy Convers. Manag. 209, 112588.

Kanner, S., Wang, L., Persson, P.O., 2016. Implicit large-eddy simulation of 2d counter-rotating vertical-axis wind turbines. In: 34th Wind Energy Symposium, p. 1731.

Lam, H.F., Peng, H.Y., 2017. Measurements of the wake characteristics of co-and counter-rotating twin H-rotor vertical axis wind turbines. Energy 131, 13–26.

Menter, F.R., 1994. Two-equation eddy-viscosity turbulence models for engineering applications. AIAA J. 32 (8), 1598–1605.

Naik, H., Tiwari, S., 2021. Thermodynamic performance analysis of an inline fin-tube heat exchanger in presence of rectangular winglet pairs. Int. J. Mech. Sci. 193, 106148.

Ni, L., Miao, W., Li, C., Liu, Q., 2021a. Impacts of Gurney flap and solidity on the aerodynamic performance of vertical axis wind turbines in array configurations. Energy 215, 118915.

Ni, L., Miao, W., Li, C., Liu, Q., 2021b. Impacts of Gurney flap and solidity on the aerodynamic performance of vertical axis wind turbines in array configurations. Energy 215, 118915.

Patankar, S.V., 1980. Numerical Heat Transfer and Fluid Flow. Hemisph Publ Corp, Washington DC.

Peng, H.Y., Han, Z.D., Liu, H.J., Lin, K., Lam, H.F., 2020. Assessment and optimization of the power performance of twin vertical axis wind turbines via numerical simulations. Renew. Energy 147, 43–54.

Posa, A., 2019. Wake characterization of coupled configurations of vertical axis wind turbines using Large Eddy Simulation. Int. J. Heat Fluid Flow 75, 27–43.

January Raciti Castelli, M., Ardizzon, G., Battisti, L., Benini, E., Pavesi, G., 2010. Modeling strategy and numerical validation for a Darrieus vertical axis micro-wind turbine. ASME Int. Mech. Eng. Congress Exposit. 44441, 409–418.

Rezaeiha, A., Kalkman, I., Blocken, B., 2017. Effect of pitch angle on power performance and aerodynamics of a vertical axis wind turbine. Appl. Energy 197, 132–150.

Rezaeiha, A., Montazeri, H., Blocken, B., 2018a. Characterization of aerodynamic performance of vertical axis wind turbines: impact of operational parameters. Energy Convers. Manag. 169, 45–77.

Rezaeiha, A., Montazeri, H., Blocken, B., 2018b. Characterization of aerodynamic performance of vertical axis wind turbines: impact of operational parameters. Energy Convers. Manag. 169, 45–77.

Roache, P.J., 1997a. Quantification of uncertainty in computational fluid dynamics. Annu. Rev. Fluid Mech. 29 (1), 123–160.

Roache, P.J., 1997b. Quantification of uncertainty in computational fluid dynamics. Annu. Rev. Fluid Mech. 29 (1), 123–160.

Sahebzadeh, S., Rezaeiha, A., Montazeri, H., 2020. Towards optimal layout design of vertical-axis wind-turbine farms: double rotor arrangements. Energy Convers. Manag. 226, 113527.

Simcenter, S.C., 2018. Version 13.06. Siemens PLM Software: Plano, TX, USA.

Su, J., Chen, Y., Han, Z., Zhou, D., Bao, Y., Zhao, Y., 2020a. Investigation of V-shaped blade for the performance improvement of vertical axis wind turbines. Appl. Energy 260, 114326.

Su, J., Chen, Y., Han, Z., Zhou, D., Bao, Y., Zhao, Y., 2020b. Investigation of V-shaped blade for the performance improvement of vertical axis wind turbines. Appl. Energy 260, 114326.

Wilcox, D.C., 1998. Turbulence Modelling for CFD, 2. DCW industries La Canada, CA.

Yang, Y., Guo, Z., Song, Q., Zhang, Y., Li, Q.A., 2018. Effect of blade pitch angle on the aerodynamic characteristics of a straight-bladed vertical axis wind turbine based on experiments and simulations. Energies 11 (6), 1514.

Zanforlin, S., Nishino, T., 2016. Fluid dynamic mechanisms of enhanced power generation by closely spaced vertical axis wind turbines. Renew. Energy 99, 1213–1226.